VSP

Advanced Composite Materials 17 (2008) 75–87

ADVANCED COMPOSITE MATERIALS
www.brill.nl/acm

High Temperature Fiber Fragmentation Characteristics of SiC Single-Fiber Composite With Titanium Matrices

Theodore E. Matikas *

Department of Materials Science and Engineering, University of Ioannina, University Campus, 45110 Ioannina, Greece

Received 5 March 2007; accepted 2 July 2007

Abstract

Aerospace structural applications, along with high performance marine and automotive applications, require high-strength efficiency, which can be achieved using metal matrix composites (MMCs). Rotating components, such as jet-engine blades and gas turbine parts, require materials that maximize strength efficiency and metallurgical stability at elevated temperatures. Titanium matrix composites (TMCs) are well suited in such applications, since they offer an enhanced resistance to temperature effects as well as corrosion resistance, in addition to optimum strength efficiency. The overall behavior of the composite system largly depends on the properties of the interface between fiber and matrix. Characterization of the fiber–matrix interface at operating temperatures is therefore essential for the developemt of these materials. The fiber fragmentation test shows good reproducibility of results in determining interface properties.

This paper deals with the evaluation of fiber fragmentation characteristics in TMCs at elevated temperature and the results are compared with tests at ambient temperature. It was observed that tensile testing at 650°C of single-fiber TMCs led to limited fiber fragmentation behavior. This indicates that the load transfer from the matrix to the fiber occurs due to interfacial friction, arising predominantly from mechanical clamping of the fiber by radial compressive residual and Poisson stresses. The present work also demonstrates that composite processing conditions can significantly affect the nature of the fiber–matrix interface and the resulting fragmentation of the fiber.

Keywords

Titanium, metal matrix composites, fiber–matrix interface, fiber fragmentation

1. Introduction

The anisotropic nature of fiber reinforced composites necessitates the optimization of interface properties. Thus, the requirement of a strong interface for adequate transverse strength and creep resistance is at variance with the conventional wisdom of a weak interface for longitudinal strength. In the absence of a matrix crack the

* E-mail: matikas@otenet.gr
Edited by the JSCM and KSCM

 DOI:10.1163/156855108X295663

interface becomes important only in the presence of a fiber break. Fairly high shear and compressive radial stresses are generated at the interface next to the break [1, 2], and the former can be sufficient to cause interface shear failure and relative fiber–matrix sliding.

Various techniques are currently available for quantifying the interfacial properties of metal matrix composites. In particular, test methods for measuring the interfacial shear properties of continuously reinforced MMCs include the thin slice fiber push-out, fiber pull-out, transverse, and fiber fragmentation tests. The fiber fragmentation test was developed by Kelly and Tyson [3], who investigated the behavior of brittle tungsten fibers embedded in a copper matrix composite specimen under tension. Elongating the specimens in tension results in fiber breakage into multiple segments. The fiber inside the matrix breaks into increasingly smaller fragments at locations where the axial stress of the fiber reaches its tensile strength. When the fiber breaks, the tensile stress at the location of fracture reduces to zero. Due to the constant shear in the matrix, the tensile stress in the fiber increases almost linearly from its ends to a plateau in longer fragments. The higher the axial strain applied, the more fractures will be caused in the fiber, but at some level the number of breaks will become constant as the fragment length is too short to transfer enough stress from the matrix to the fiber to cause further fragmentation.

Although the single-fiber fragmentation test was first performed on MMCs during the early 1960s [3], the subsequent application of this test was primarily limited to transparent polymer composites due to the ease of their preparation and observation of the fiber fragments using birefringence techniques [4–12]. There has been an interest, however, in the application of this test to model metal matrix composites using various techniques [13–21]. Ochiai and Osamura [13] tested a number of single W fiber-reinforced Cu matrix composite specimens with different thickness and showed that the average fragment length increased with increasing volume fraction of the fiber. The work of Roman and Aharonov dealt with the fiber fragmentation in Al matrix composites reinforced with different types of silicon carbide fibers and showed that the friction arising from thermal residual stresses plays a major role in determining the interfacial shear stresses in these composites [14]. Molliex *et al.* [15] studied fragmentation in SCS-2 fiber-reinforced Al alloy composites and concluded that interfacial stress transfer in these materials is limited by the plastic deformation of the matrix alloy. Clough *et al.* [16] and Houpert *et al.* [17] conducted single fiber fragmentation tests on SiC fiber-reinforced single crystal aluminum and Al_2O_3 fiber-reinforced copper matrix composites, respectively, and analyzed the results in terms of the load drops corresponding to fiber fragmentation.

Studies dealing with fiber fragmentation in titanium-based composites are limited. Vassel *et al.* [15, 18] and Le Petitcorps *et al.* [19] conducted single fiber fragmentation tests on Ti-6Al-4V matrix composites containing different types of SiC fibers. Favre *et al.* [20] reported the occurrence of load drops corresponding to fiber fragmentation in a few SCS-6/Ti-14Al-21Nb (wt%) composite specimens tensile tested at 425°C. These past studies were concerned mainly with the estima-

tion of the interfacial shear strength using the observed fragment length data. The present study of fiber fragmentation in titanium-based composites aims at understanding the influence of interface microstructure and constituent properties on the shear load transfer and fiber fragmentation. This paper undertakes to determine the effects of fiber–matrix interfacial reaction, residual strain and matrix deformation characteristics on high temperature fiber fragmentation behavior.

2. Experimental

2.1. Processing of Single-Fiber Composites

Two different composite systems were used in this work, Ti-6Al-4V/SCS-6 and Ti-14Al-2lNb/SCS-6. Single-fiber composite (SFC) samples were fabricated by diffusion bonding of a fiber placed between matrix alloy sheets at temperatures below the β transus of the alloys using two different processing routes: (I) a two-step process involving vacuum hot pressing at 925°C under 5.5 MPa pressure for 30 min followed by hot isostatic pressing at 985°C under 100 MPa pressure for 2 h, and (II) a single-step consolidation process involving vacuum hot pressing at 954°C under a pressure of 9.2 MPa for 30 min. The composite panels fabricated by these two routes are designated as Type I (two-step process) and Type II (single-step process) samples.

All composite panels were subjected to ultrasonic nondestructive evaluation using shear and longitudinal wave interrogations in order to determine the quality of their consolidation. Metallographic sections were taken normal to the fiber axis to examine the fiber–matrix interface region. The consolidated composite panels were machined into 1.5 mm thick dog-bone type tensile specimens with 19.0 mm × 6.4 mm gage sections having a fiber volume fraction of ∼0.16%. All test specimens were examined by microfocus X-ray radiography to ascertain proper alignment of the fiber parallel to the tensile specimen axis.

2.2. Mechanical Testing

Tensile tests were conducted on a servohydraulic machine in laboratory air both at room temperature and at 650°C using a nominal strain rate of 2×10^{-4}/s for Ti-6Al-4V/SCS-6 and 1×10^{-4}/s for Ti-14Al-2lNb/SCS-6 specimens. The results reported here are based on test data from at least two specimens in each microstructural condition. Tensile loading was continued until fracture of the specimen in most of the tests. A few tests were interrupted at intermediate strains to determine the evolution of fragmentation as a function of specimen strain.

2.3. Acoustic Emission Monitoring

Acoustic emission activity was monitored during tensile testing by employing a broadband resonant transducer with a nominal center frequency of 250 kHz (MICRO 30, Physical Acoustic Corporation — PAC), which was coupled *via* high vacuum grease to the flat gage section of the samples. Transducer outputs were

amplified first by 40 dB using a preamplifier (Model 1220A, PAC) with a band-pass filter of 100–400 kHz and then by an additional 20 dB at the main amplifier (Locan AT, PAC). Acoustic emission waveform parameters, as well as appropriate stress, strain and RMS voltage of the amplified transducer outputs were recorded by a computerized data acquisition system.

2.4. Ultrasonic Nondestructive Evaluation

The embedded fiber in the composites was ultrasonically imaged using longitudinal and shear wave interrogations to access the consolidation of composite specimens and to monitor the fiber fragmentation behavior following tensile testing. In the longitudinal wave technique, a 50 MHz focused transducer (6.3 mm diameter, 25.4 mm focal length) was used in the pulse-echo mode with the wave front normal to the specimen surface. Under this condition, a compressional wave was propagated in the matrix, and was reflected from the fiber back to the transducer. In the shear wave technique, a 25 MHz focused transducer (6.3 mm diameter, 12.7 mm focal length) was used in the pulse-echo mode and the ultrasonic wave front was incident on the specimen surface inclined to the vertical plane at an angle of either 18° or 24°. Since these angles lie between the first and the second critical angle, only vertically polarized shear waves propagated in the matrix and were incident on the fiber–matrix interface. Further details of the application of these ultrasonic techniques can be found elsewhere [22, 23].

3. Results and Discussion

3.1. Microstructure of the Interface Region

The fiber–matrix interfacial regions of Ti-6Al-4V/SCS-6 and Ti-14Al-2lNb/SCS-6, Type I single-fiber composites are shown in Fig. 1. The Ti-6Al-4V/SCS-6 system exhibited a significant reaction zone with a very rough interface, which was produced due to preferential reaction between the β-phase of the matrix alloy and the carbon-rich coating layers of the fiber. As Fig. 1 shows, this reaction zone is composed of two layers with non-uniform thickness. Much of the outer, carbon-rich layer of the SCS-6 fiber coating was consumed by this reaction, and a part of its inner, carbon-rich layer, was also attacked by the matrix at several locations along the fiber (Fig. 2). In contrast, the Ti-14Al-2lNb/SCS-6 composite showed a narrower and smoother interfacial reaction zone. However, this composite also showed a wide region of the matrix adjacent to the fiber was devoid of the β phase.

The consolidation of Type II Ti-6Al-4V/SCS-6 composite samples was nearly complete and only small voids remained near the junction of the fiber and the bonding surfaces of the sheets. Figure 3 shows the fiber–matrix interface regions of two such samples and illustrates the reproducibility of the microstructure. The size of the remnant voids was observed to differ slightly from sample to sample as seen in these micrographs. In comparison to the Type I samples, the Type II Ti-6Al-4V/SCS-6 composite showed a significantly smoother fiber–matrix interface. On

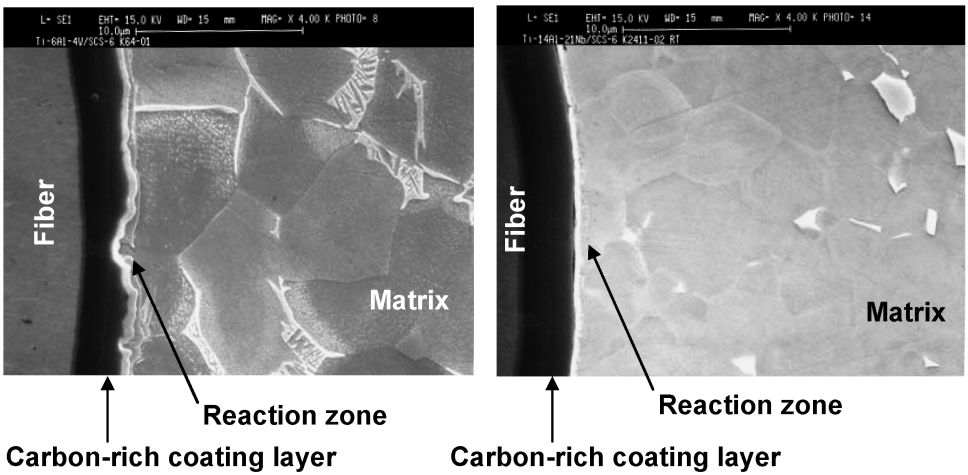

Figure 1. SEM micrographs showing the fiber–matrix interphase region of Type I single-fiber composites consolidated using the two-step process: (a) Ti-6Al-4V/SCS-6 and (b) Ti-14Al-21Nb/SCS-6.

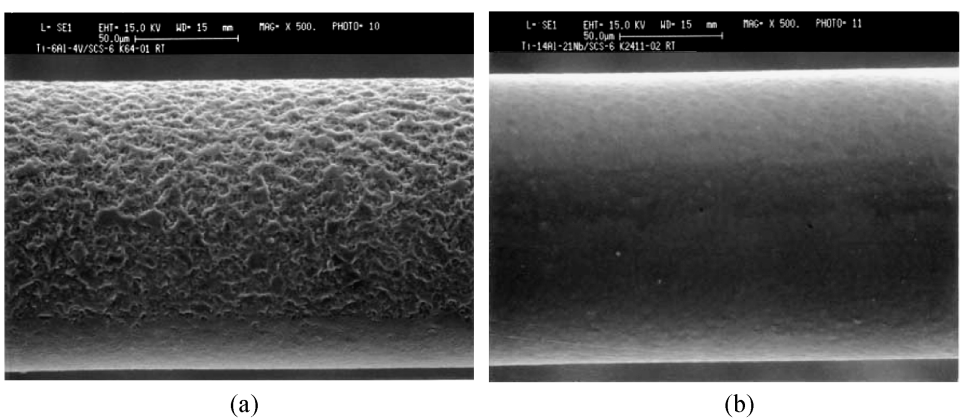

Figure 2. SEM micrographs showing the surface of fiber extracted from Type I single-fiber composites tensile tested at room temperature: (a) Ti-6Al-4V/SCS-6 and (b) Ti-14Al-21Nb/SCS-6.

the other hand, the single step processing was inadequate for achieving full consolidation of the Ti-14Al-2lNb/SCS-6 composite.

3.2. Fiber Fragmentation Testing at Room Temperature

Typical room temperature tensile stress–strain curves for the Ti-6Al-4V/SCS-6 and Ti-14Al-2lNb/SCS-6, Type I single-fiber composites, which were consolidated by the two-step process, are shown in Fig. 4. The variation of the acoustic emission amplitude with strain is also shown. The Ti-6Al-4V/SCS-6 specimens displayed continuous yielding with high values of yield strength and elongation. This stress–strain behavior is consistent with the published tensile data for this alloy in the equiaxed

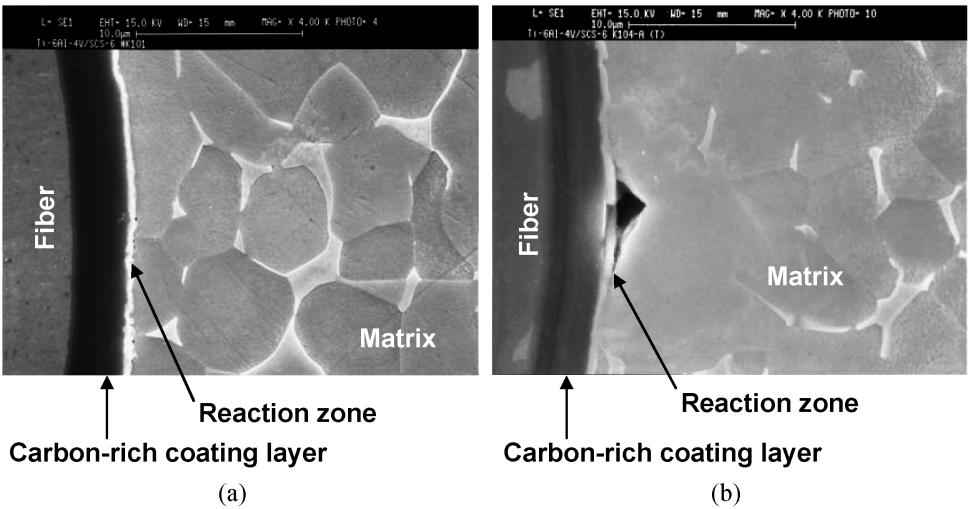

Figure 3. SEM micrographs showing the fiber–matrix interphase region of two Type II Ti-6Al-4V/SCS-6 single-fiber composites consolidated using the one-step process: (a) Fully consolidated and (b) with remnant defects.

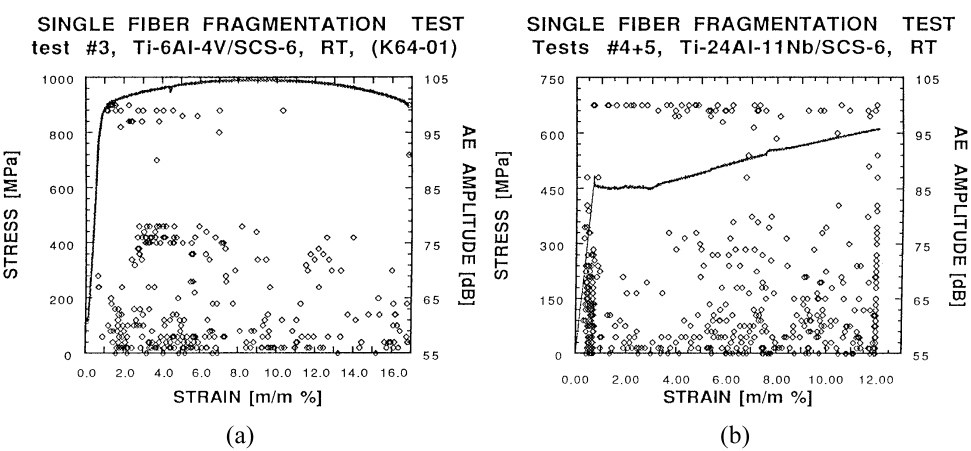

Figure 4. Tensile stress–strain behavior and acoustic emission amplitude *vs* strain for the Type I single-fiber composites tested at room temperature: (a) Ti-6Al-4V/SCS-6 and (b) Ti-14Al-21Nb/SCS-6.

$(\alpha + \beta)$ microstructural condition. The Ti-14Al-21Nb/SCS-6 specimens exhibited a distinct yield point, yield drop and Luder's band formation, and deformed at much lower flow stresses as compared to the Ti-6Al-4V/SCS-6 composites.

After the fragmentation testing, the specimens were sectioned and polished parallel to the fiber axis using standard metallographic specimen preparation techniques. Metallographic examination of the fibers in Type I composites revealed distinctly different fiber fracture behavior in the two composite systems. The fiber fragments in Ti-14Al-2lNb/SCS-6 were significantly longer than those in Ti-6Al-

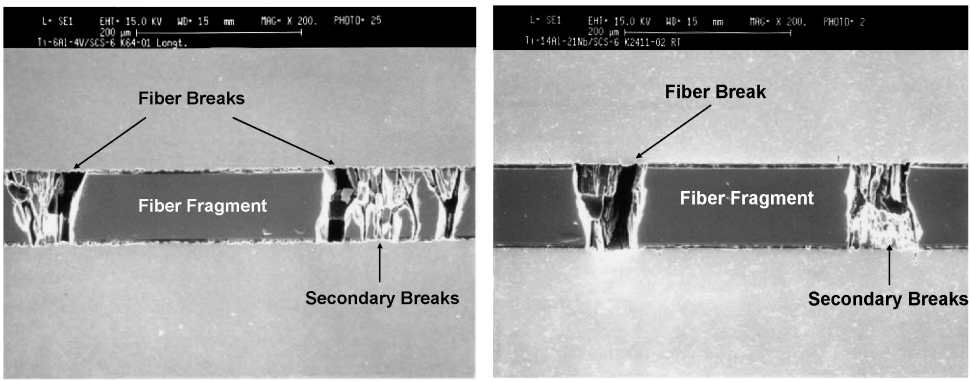

(a) (b)

Figure 5. SEM micrographs showing details of fiber fracture, reaction zone cracking and interface region following tensile testing at room temperature of: (a) Ti-6Al-4V/SCS-6 SFC and (b) Ti-14Al-21Nb/SCS-6 SFC.

4V/SCS-6. Both the composites revealed the presence of several short, secondary fiber ruptures between the longer primary fragments (Fig. 5). The distinction between primary and secondary fiber ruptures using metallography was more difficult in the case of Ti-6Al-4V/SCS-6 since the fragmentation occurred on a finer scale and resulted in severe shattering of the fiber with numerous secondary ruptures. The primary and secondary fractures could also be distinguished on the basis of acoustic emission amplitude and event duration, with the primary fractures corresponding to high dB levels and long durations, and the secondary fiber cracking corresponding to low dB levels and short durations. On the basis of the AE characteristics of fiber fractures, it is observed that fragmentation attains saturation in the Ti-6Al-4V/SCS-6 Type I specimens. The reason for achieving saturation in Ti-6Al-4V Type I SFC is the severity of the fiber–matrix reaction and interface roughness causing extensive fracture. This is not the case in the Type II Ti-6Al-4V. On the other hand, Ti-14Al-2lNb/SCS-6 composites do not attain saturation of fiber fragmentation. The occurrence of fragmentation is closely related to the work hardening rate of the matrix material, since the fiber loading continues if the work hardening rate is high. Ti-14Al-21Nb/SCS-6 exhibits higher work hardening rate past yield than Ti-6Al-4V/SCS-6, which results in continued occurrence of high amplitude AE events in Ti-14Al-2lNb/SCS-6 samples, indicating that fiber fragmentation does not saturate in this case. The different behavior of Ti-6Al-4V/SCS-6 and Ti-14Al-21Nb/SCS-6 composites in terms of fragmentation saturation can be observed in Fig. 6, which shows the frequency of occurrence of fiber fractures with increasing strain in the two composite systems.

3.3. Fiber Fragmentation Testing at 650° C

Fiber fragmentation tests indicate that load is transferred from the matrix to the fiber, primarily by frictional stresses. The friction between the fiber and matrix dur-

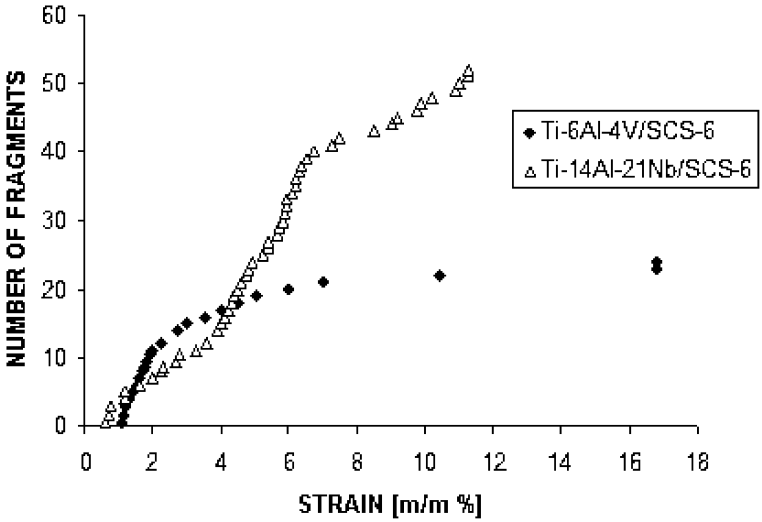

Figure 6. Number of fragments *vs* strain in single fiber fragmentation test of Ti-6Al-4V/SCS-6 and Ti-14Al-21Nb/SCS-6 single-fiber composites tested at room temperature.

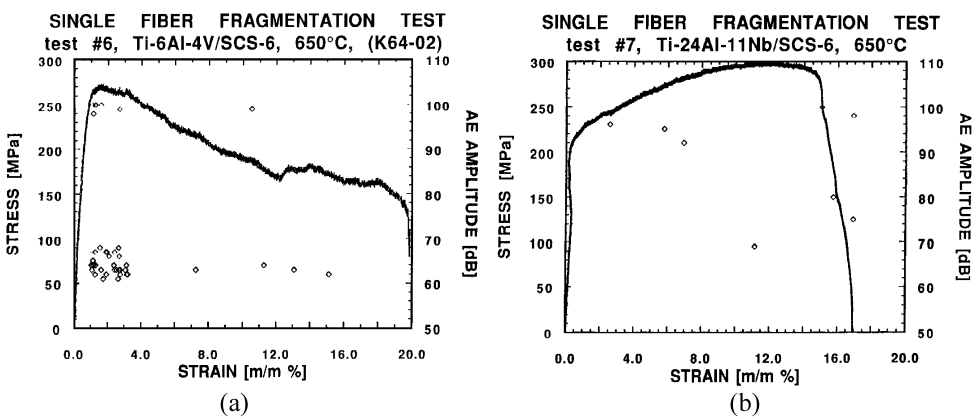

Figure 7. Tensile stress–strain and acoustic emission amplitude *vs* strain curves for the Type I single-fiber composites tested at 650°C: (a) Ti-6Al-4V/SCS-6 and (b) Ti-14Al-21Nb/SCS-6.

ing loading of the composite is due to residual compressive thermal stresses, which result from the temperature difference between consolidation and testing temperatures, and the difference between the thermal expansion coefficients of the fiber and matrix.

Tensile stress–strain curves for Ti-6Al-4V/SCS-6 and Ti-14Al-2lNb/SCS-6, Type I single-fiber composites tested at 650°C are shown in Fig. 7. The variation of acoustic emission amplitude with strain is also shown. The number and length of the fragments in the Ti-6Al-4V/SCS-6 composite was measured using metallography (Fig. 8). It was found that the number of fragments increases with the

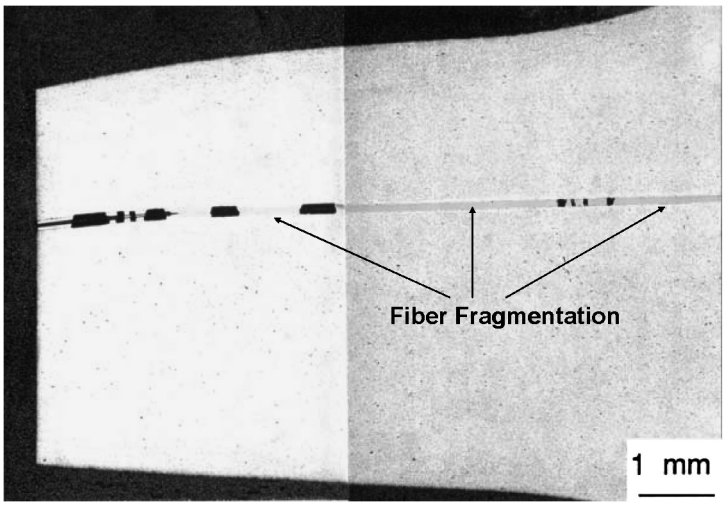

Figure 8. Optical micrograph showing fiber fragmentation in Ti-6Al-4V/SCS-6, Type I single-fiber composite tested at 650°C.

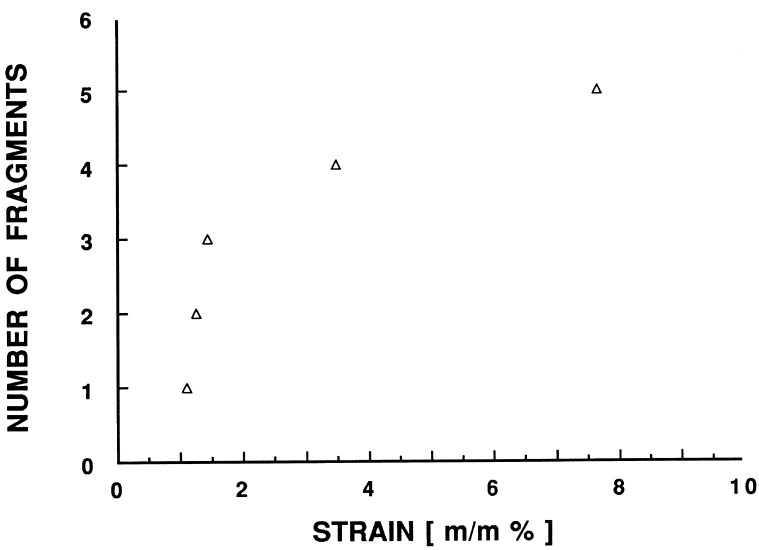

Figure 9. Number of fragments *vs* strain in single-fiber fragmentation test of Ti-6Al-4V/SCS-6 single-fiber composite tested at 650°C.

increasing of the fiber–matrix reaction. However, fewer fragments were found in all cases tested at 650°C, with an average fragment length in the order of 150 μm for a Ti-6Al-4V/SCS-6 single-fiber composite tested at ambient temperature, compared to about 1000 μm in the case of the same composite system tested at 650°C. Figure 9 shows the frequency of occurrence of fiber fractures with increasing strain in the Ti-6Al-4V/SCS-6 composite system tested at 650°C. Comparing Figs 6 and 9, it

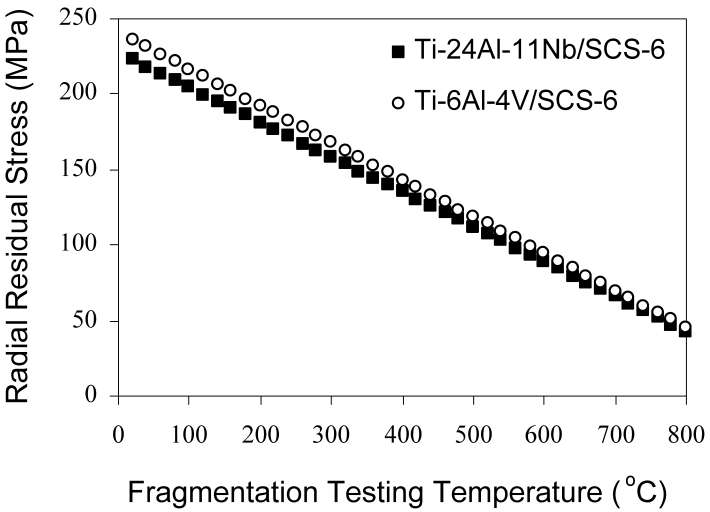

Figure 10. Radial compressive residual stresses *vs* testing temperature for two different composite systems, Ti-14Al-21Nb/SCS-6 and Ti-6Al-4V/SCS-6.

becomes evident that the number of fragments for the Ti-6Al-4V/SCS-6 composite system tested at high temperature (650°C) was found almost four times lower than the number of fragments for the same composite system tested at room temperature.

This can be explained by the fact that, when the fiber fragmentation test is done at higher temperatures, the relaxation of residual stresses dominates the fragmentation phenomenon. Figure 10 shows the state of the compressive radial residual stresses for two different composite systems, Ti-14Al-21Nb/SCS-6 and Ti-6Al-4V/SCS-6, as a function of the temperature at which the fiber fragmentation test is performed. By comparing tests in Fig. 10 performed at room temperature (RT) with those at high temperature (HT) it can be observed that, in the case of a testing temperature of 650°C, residual stresses are reduced by a factor of three.

Using shear-lag analysis [3], the average shear strength of the fiber–matrix interface can be estimated as a function of the average critical fragment length of the fiber. Figure 11 shows the relationship between the interfacial shear strength and the average fragment length for a composite with a single SCS-6 fiber. From Fig. 11, and taking into account the measured average fragment lengths for a Ti-6Al-4V/SCS-6 single-fiber composite tested both at room temperature and at 650°C, which were about 150 μm and 1000 μm, respectively, it is estimated that the average shear strength of the fiber–matrix interface is in the order of 1 GPa and 150 MPa for operating temperatures of 23°C and 650°C, respectively.

4. Conclusions

The present study showed a distinctly different fiber fragmentation behavior in Ti-6Al-4V/SCS-6 and Ti-14Al-2INb/SCS-6 composites, caused by differences in the fiber–matrix interfacial region. Fragmentation characteristics are significantly

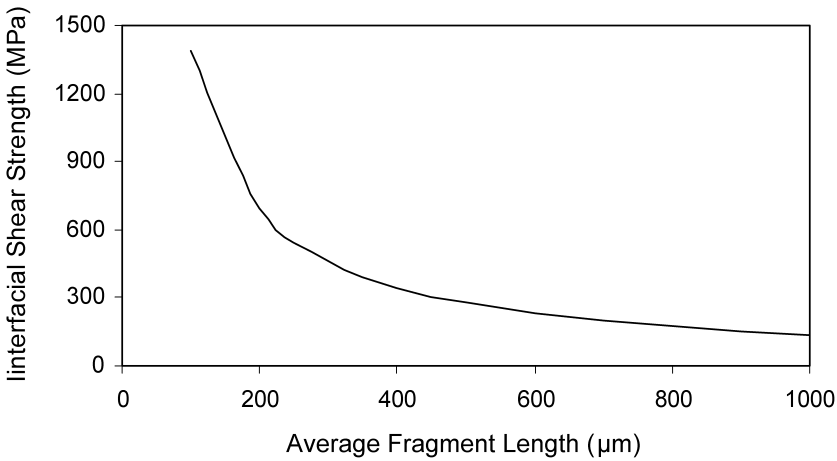

Figure 11. Average fiber–matrix interface shear strength *vs* average fragment length for a single SCS-6 fiber composite.

affected by fiber–matrix reaction. Defects produced by this reaction at the fiber surface can lead to reduced fiber strength and result in extensive fragmentation of the fiber. This is influenced by matrix alloy composition as well as processing conditions.

It was also observed that the interfacial properties of silicon carbide fibers are primarily influenced by friction. In addition, it was found that the normal (clamping) forces at the interface scale with the yield strength of the matrix, suggesting that the magnitude of work-hardening in the matrix is an important property to consider in the fragmentation process. This may help to explain the observation in Ti-alloy specimens that fragmentation continues till specimen failure, rather than reaching saturation, as often observed in composites with low work-hardening rate, such as Cu.

This study has further shown that the evolution of fragmentation is related to the stress–strain characteristics of the matrix alloy. The onset of fragmentation is related to the residual strain in the fiber. The influence of residual strain on the fragmentation behavior is supported by results from fiber fragmentation testing performed at higher temperatures. It was clearly observed that fewer fragments occur at elevated tempertures, indicating that the relaxation of residual stresses at these temperatures dominates the fiber fragmentation process. Finally, the average shear strength of the fiber–matrix interface was estimated to drop by almost a factor of seven when the composite was tested at 650°C, compared to testing performed at ambient temperature.

Acknowledgements

The assistance of Dr. S. Krishnamurthy in conducting the experiments is acknowledged. The results of NDE and AE work reported here are part of a collaborative effort between the author and Drs. I. Roman and M. C. Waterbury.

References

1. M. J. Iremonger and W. G. Wood, Plastic flow and failure of discontinuous-fibre composite materials, *J. Strain Anal.* **5**, 212–222 (1970).
2. A. S. Carrara and F. J. McGarry, Matrix and interface stresses in a discontinuous fiber composite model, *J. Compos. Mater.* **2**, 222–243 (1968).
3. A. Kelly and W. R. Tyson, Tensile properties of fiber-reinforced metals: copper/tungsten and copper/molybdenum, *J. Mech. Phys. Solids* **3**, 329–350 (1965).
4. J.-P. Favre and D. Jacques, Stress transfer in carbon fibre model composites, *J. Mater. Sci.* **25**, 1373–1380 (1990).
5. M. C. Waterbury and L. T. Drzal, On the determination of fiber strengths by *in-situ* fiber strength testing, *J. Compos. Tech. Res.* **13**, 22–28 (1991).
6. M. Narkis, E. J. H. Chen and R. B. Pipes, Review of methods for characterization of interfacial fiber–matrix interactions, *Polym. Compos.* **9**, 245–251 (1988).
7. R. B. Henstenburg and S. L. Phoenix, Interfacial shear strength studies using the single-filament-composite test. Part II: A probability model and Monte Carlo simulation, *Polym. Compos.* **10**, 389–408 (1989).
8. L. T. Drzal, M. Rich and P. Lloyd, Adhesion of graphite fibers to epoxy matrices. I. The role of fiber surface treatment, *J. Adhesion* **16**, 1–30 (1983).
9. W. A. Fraser, F. H. Ancker, A. T. DiBenedetto and B. Elbirli, Evaluation of surface treatments for fibers in composite materials, *Polym. Compos.* **4**, 238–248 (1983).
10. A. N. Netravali, R. B. Henstenburg, S. L. Phoenix and P. Schwartz, Interfacial shear strength studies using the single-filament-composite test. Part I: Experiments on graphite fibers in epoxy, *Polym. Compos.* **10**, 226–241 (1989).
11. F. G. Torres and M. L. Cubillas, Study of the interfacial properties of natural fibre reinforced polyethylene, *Polymer Testing* **24**, 694–698 (2005).
12. X.-M. Li, J.-H. Wang, G.-Q. Gao and W. Feng, Study on the interfacial adhesion conditions by single-fiber composite fragmentation test, *Wuhan Ligong Daxue Xuebao/J. Wuhan University of Technology* **27**, 9–12 (2005).
13. S. Ochiai and K. Osamura, Multiple fracture of a fibre in a single tungsten fibre–copper matrix composite, *Z. Metallkd.* **77**, 255–259 (1986).
14. I. Roman and R. Aharonov, Mechanical interrogation of interfaces in monofilament model composites of continuous SiC fiber–aluminum matrix, *Acta Metall. Mater.* **40**, 477–485 (1992).
15. L. Molliex, J.-P. Favre, A. Vassel and M. Rabinovitch, Interface contribution to the SiC–titanium and SiC–aluminium tensile strength prediction, *J. Mater. Sci.* **29**, 6033–6040 (1994).
16. R. B. Clough, F. S. Biancaniello, H. N. G. Wadley and U. R. Kattner, Fiber and interface fracture in single crystal aluminum/SiC fiber composites, *Metall. Trans.* **21A**, 2747–2757 (1990).
17. J.-L. Houpert, S. L. Phoenix and R. Raj, Analysis of the single-fiber-composite test to measure the mechanical properties of metal–ceramic interfaces, *Acta Metall. Mater.* **42**, 4177–4187 (1994).
18. A. Vassel, M. C. Merienne, F. Pautonnier, L. Molliex and J.-P. Favre, A method to evaluate the bonding between fibre and matrix in Ti-base composite, in: *Proc. 6th World Conference on Titanium*, P. Lacombe, R. Tricot and G. Beranger (Eds), pp. 919–923. Les Editions de Physique, Les Ulis Cedex, France (1988).
19. Y. Le Petitcorps, R. Pailler and R. Naslain, The fibre/matrix interfacial shear strength in titanium alloy matrix composites reinforced by silicon carbide or boron CVD filaments, *Compos. Sci. Technol.* **35**, 207–214 (1989).
20. J.-P. Favre, A. Vassel and C. Laclau, Testing of SiC/titanium composites by fragmentation and push-out tests: comparison and discussion of test data, *Composites* **25**, 482–487 (1994).

21. M. Preuss, G. Rauchs, P. J. Withers, E. Maire and J.-Y. Buffiere, Interfacial shear strength of Ti/SiC fibre composites measured by synchrotron strain measurement, *Composites, Part A* **33**, 1381–1385 (2002).
22. S. Krishnamurthy, T. E. Matikas, P. Karpur and D. B. Miracle, Ultrasonic evaluation of the processing of fiber-reinforced metal–matrix composites, *Compos. Sci. Technol.* **54**, 161–168 (1995).
23. M. C. Waterbury, P. Karpur, T. E. Matikas, S. Krishnamurthy and D. B. Miracle, *In situ* observation of the single fiber fragmentation process in metal matrix composites by ultrasonic imaging, *Compos. Sci. Technol.* **52**, 261–266 (1994).